tm – Technisches Messen 2019; 86(12): 758–764 DE GRUYTER OLDENBOURG

Maximilian Schambach* and Fernando Puente León

Reconstruction of multispectral images from spectrally coded light fields of flat scenes

Rekonstruktion multispektraler Bilder aus spektral codierten Lichtfeldern flacher Szenen

https://doi.org/10.1515/teme-2019-0103
Received July 12, 2019; accepted August 2, 2019

Abstract: We present a novel method to reconstruct multispectral images of flat objects from spectrally coded light fields as taken by an unfocused light field camera with a spectrally coded microlens array. In this sense, the spectrally coded light field camera is used as a multispectral snapshot imager, acquiring a multispectral datacube in a single exposure. The multispectral image, corresponding to the light field's central view, is reconstructed by shifting the spectrally coded subapertures onto the central view according to their respective disparity. We assume that the disparity of the scene is approximately constant and non-zero. Since the spectral mask is identical for all subapertures, the missing spectral data of the central view will be filled up from the shifted spectrally coded subapertures. We investigate the reconstruction quality for different spectral masks and camera parameter sets optimized for real life applications such as in-line production monitoring for which the constant disparity constraint naturally holds. For synthesized reference scenes, using 16 color channels, we achieve a reconstruction PSNR of up to 51 dB.

Keywords: Multispectral imaging, light fields.

Zusammenfassung: Wir präsentieren eine neuartige Methode zur Rekonstruktion von multispektralen Bildern flacher Objekte aus spektral codierten Lichtfeldern, wie sie mit einer Lichtfeldkamera mit spektral kodiertem Mikrolinsenarray aufgenommen werden. In diesem Sinne entspricht die spektral codierte Lichtfeldkamera einer multispektralen Snapshot Kamera. Das der Zentralansicht des Lichtfelds entsprechende multispektrale Bild wird rekonstruiert, indem die spektral codierten Subapertur-Bilder, abhängig von der jeweiligen Disparität, auf die Zentralansicht transformiert werden. Wir nehmen an, dass die Disparität der Szenen konstant und ungleich null ist. Da die spektrale Kodierung für alle Subapertur-Bilder identisch ist, wird die fehlende spektrale Information jedes Pixels der Zentralansicht von den transformierten spektral kodierten Subapertur-Bildern aufgefüllt. Wir untersuchen die Qualität der Rekonstruktion für verschiedene Masken der spektralen Kodierung und Kameraparameter, welche für echte Anwendungen, wie beispielsweise der Produktionsüberwachung, welche die Auflage einer konstanten Disparität auf natürliche Art erfüllen, angepasst sind. Mithilfe synthetischer Referenzdaten, im Falle von 16 Farbkanälen, erreichen wir eine Rekonstruktionsqualität von bis zu 51 dB.

Schlagwörter: Multispektrale Bildgebung, Lichtfelder.

1 Introduction

In recent years, multispectral snapshot as well as light field imaging systems have gained a lot of attention in both scientific research and industrial applications. Multispectral cameras capture a spatially resolved spectrum of a scene using several spectral bands (typically up to 30). Multispectral images can then for example be used to enhance image-based classification in sorting tasks [12, 16], medical diagnostics [11] or to estimate material abundances [10, 2]. As opposed to scanning techniques, snapshot cameras are able to record non-static scenes. Light field cameras, on the other hand, capture a multi-angle view of a scene, usually only utilizing three color channels. Light fields then provide depth information [18] which can for example be used for 3-D shape reconstruction [17]. As a compact monocular camera, microlens array (MLA) based light field cameras [1] are the most practical light field cameras in non-lab scenarios. Not only do they offer a compact and robust way for depth estimation, but due to their optical design make it possible to obtain a high depth-of-field with small f-numbers, i. e. they are good candidates for low light and non-static scenes.

Recently, some effort has been made to record multi- or hyperspectral light fields. The *spectral 4D light field*

***Corresponding author: Maximilian Schambach,** Karlsruhe Institute of Technology, Institute of Industrial Information Technology, Karlsruhe, Germany, e-mail: schambach@kit.edu, ORCID: https://orcid.org/0000-0002-4927-266X
Fernando Puente León, Karlsruhe Institute of Technology, Institute of Industrial Information Technology, Karlsruhe, Germany

$L(u,v,s,t;\lambda)$ describes the optical radiance along a ray parameterized by (u,v,s,t) at wavelength λ at a given moment in time (here, we consider only the static case and do not specifically denote a time variable). In the case of monocular computational cameras, one usually uses the plane-plane ray parametrization, i. e. a ray inside a camera is uniquely defined by the intersection points of two parallel planes: the (u,v)- and the (s,t)-plane (usually, the main lens and MLA plane). While the (s,t)-coordinate indexes the spatial dependency of the light field, the (u,v)-coordinate represents the angular dependency.

To record a spectral 4D light field, one could use a monochromatic light field camera and a standard spectral scanning approach: By placing narrow bandpass filters in front of the camera, the spectral 4D light field is captured channelwise. As a snapshot imaging system, beside multi-camera approaches [19, 23], there are basically only two possibilities: either spectrally coding the (u,v)-coordinate [8, 4] or the (s,t)-coordinate [21] of the spectral 4D light field. In the presented approach, we consider coding of the (s,t)-coordinates, i. e. spectrally coding the MLA of a light field camera in the so-called unfocused design [14] (such as Lytro cameras), as opposed to the focused plenoptic camera [13] (such as Raytrix cameras). While in principle, spectral coding of the MLA of a focused light field camera is possible, it would lead to a mixed (u,v,s,t)-coding and is not considered here. Hence, for the remainder, the term *light field camera* is used synonymously to a MLA based light field camera in the unfocused design. From the coded light field, a reconstruction of a multispectral image corresponding to the central view of the light field is performed.

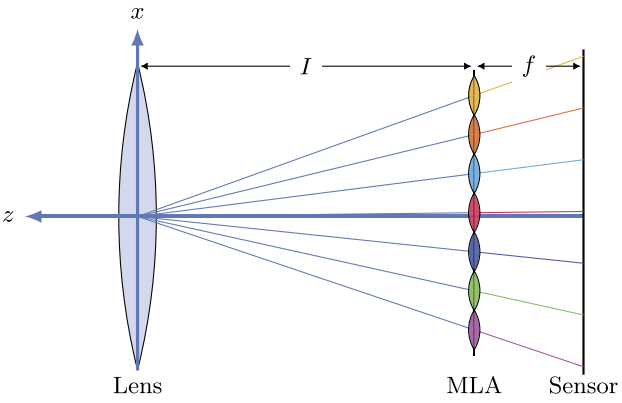

Figure 1: Light field camera with spectrally coded MLA, main lens of focal length I and ML focal length f.

2 Spectrally coded light fields

A light field camera with spectrally coded MLA (see Figure 1) captures a spectrally coded light field

$$\hat{L}(u,v,s,t;\lambda) = M(s,t;\lambda) \cdot L(u,v,s,t;\lambda)\,, \tag{1}$$

where $M(s,t;\lambda)$ corresponds to the spectral filter mask. In the discrete case for a light field of size $(U,V,S,T,\Lambda) \in \mathbb{N}_+^5$, $M(s,t;\lambda) \in \{0,1\}^{S\times T\times\Lambda}$ is a binary mask where for every lenslet (s,t) only rays with one specific wavelength index λ can pass the filter, i. e. for every $s \in [1,S]\,, t \in [1,T]$ it holds

$$\sum_{\lambda=1}^{\Lambda} M(s,t;\lambda) = 1\,. \tag{2}$$

Note that the mask is the same for all subapertures (u,v), that is the spectral coding is independent of the incident ray's angle. For a single subaperture, the spectral domain is severely undersampled (in case of 16 color channels, only 1/16 $\approx$ 6 % of the multispectral subaperture's coefficients are measured), but taking the full light field into account, the spectral information of an object, if it has non-zero disparity, passes multiple spectral filters across the different subapertures. For example, if an object has a disparity of exactly 1 px, it will show up in the subapertures at locations (s,t) that differ by multiples of $(0,1)$, $(1,0)$. Since every (s,t) is coded by one specific filter, the object is sampled, across all available subapertures (u,v), at a wavelength index λ, depending on the filter mask $M(s,t;\lambda)$. Hence, the goal of the reconstruction is to make use of the spectral information that is spread out across the different subapertures of the coded light field. Here, we do not reconstruct the full multispectral light field $L(u,v,s,t;\lambda)$ from the spectrally coded measurement (as could be done e. g. by using methods from compressed sensing), but a multispectral image corresponding to the light field's central view $I(s,t;\lambda) = L(u_c,v_c,s,t;\lambda)$, where u_c, v_c correspond to the central view's angular indices. The undersampled spectral information of the multispectral central view can be severely enhanced by mapping the remaining subapertures of the spectrally coded light field onto the central view. That is, we shift every coded subaperture $\hat{I}_{uv}(s,t;\lambda) = \hat{L}(u,v,s,t;\lambda)$ onto the central view, depending on each pixel's disparity. In this case, the disparity of the scene has to be known. Unfortunately, with standard methods, such as depth-from-epipolar-plane-images using the 2-D structure tensor [18] or slope fitting methods [22], disparity calculation is not directly possible on the spectrally coded light fields. Therefore, we will consider only scenes with (approximately) constant disparity, which has to be known for the reconstruction. For example, this is applicable in production line monitoring (flat

objects placed on a conveyor belt or lab table). Knowing the disparity, we can shift every subaperture by the disparity d and its relation to the central view of the light field:

$$\hat{I}_{uv,d}(s,t;\lambda) = \hat{I}_{uv}(s + d(u-u_c), t + d(v-v_c);\lambda)\,. \quad (3)$$

Finally, to obtain a reconstruction of the central view, we sum up the shifted subapertures and normalize pixelwise:

$$I_{\text{rec}}(s,t;\lambda) = \frac{1}{n(s,t;\lambda)} \sum_{u,v} \hat{I}_{uv,d}(s,t;\lambda)\,, \quad (4)$$

where $n(s,t;\lambda)$ is the number of pixels that have been shifted onto $(s,t;\lambda)$. Depending on the filter mask and the camera parameters, there still might be undetermined pixels in (4). Here, one could perform a full 3D, spatial 2D or spectral 1D interpolation. For simplicity, and to preserve edges in the spatial domain, we perform a 1D linear interpolation in the spectral domain.

When the disparity is integer valued, (3) does not perform any interpolation and can therefore easily be implemented in a fashion capable of real time processing. On the other hand, if the disparity is zero (which is the case for the focus plane of the main lens), the reconstruction following the proposed method is not possible: the object will have a fixed (s,t) position in all subapertures and hence only one spectral sample of the object is given. Therefore, we focus the main lens of the camera to infinity. This moves the $d = 0$-plane to infinity and all objects closer to the camera will show a positive, non-zero disparity. This has the additional advantage that the light field camera can equivalently be viewed as an array of thin lens cameras with lens radius given by the light field's camera lens radius divided by the number of subaperture views per dimension. The disparity d in px between two neighboring subapertures can then be calculated to

$$d = \frac{R \cdot f}{r \cdot N \cdot g}\,, \quad (5)$$

where R is the radius and f the focal length of the main lens, r is the microlens radius and N the number of subaperture views per dimension, i. e. the number of pixels underneath every microlens per spatial direction, and g is the object distance. As usual, we assume f-number matching of the microlenses and the main lens [14].

3 Camera parameter selection

In general, according to (5), there are many ways to control the disparity of a recorded light field using the parameters R, f, r, N and of course the object distance g. Unlike the former, only g is mostly unconstrained in its range: The main lens diameter, or, more accurately, the entrance pupil of the lens, $2R$ of a commercially available lens can only be set in well defined discrete steps given by the f-number of the lens. The focal length, using a zoom lens, can be varied but not with very high accuracy. Therefore, we choose a prime lens with a fixed focal length of 50 mm and f-number F of 1.4 or 1.8 to obtain high light throughput. The microlens radius r is ideally an integer multiple of the sensor's pixel pitch and directly related to the number N of subapertures per dimension. Hence, in practice, the most accurate way to control the disparity of a recorded light field on a flat surface is the object distance. For a realistic scenario, using a 50 mm lens, we constrain the object distance to the range from 0.75 m to 1.25 m. We are then searching for all possible parameter combinations satisfying (5) with an integer valued disparity between 1 px and 7 px and number of subapertures between 5 and 15 (to have a well defined central subaperture view of the light field, we consider only odd values). Finally, the sensor size and pixel pitch are chosen according to an *ON Semiconductor Python 25K* CMOS sensor of size 5120 × 5120 px and pixel pitch of 4.5 µm. Within these constraints, we find a set of 15 possible camera parameters which are shown in detail in Section 5.

4 Ground truth data and evaluation

To quantitatively evaluate the proposed method, suitable reference data is needed. Unfortunately, there is no real world data of full multispectral light fields available (even without the constraint of a constant disparity). Therefore, we will synthesize suitable data using a raytracer capable of rendering multispectral light fields. For this, we use a self-developed fully spectral raytracer [15]. Overall, we render five different scenes: *CD*, *Colorchart*, *Concrete*, *Curry and Graffiti*, as shown in Figure 2. The scenes consist of real world multispectral images (CD, lemons, colorcharts, concrete wall, graffiti) taken from publicly available datasets [20, 3], self-made multispectral images (curry powder) as well as RGB images (rubber surface), which in the rendering process are converted to spectral images, and synthetically defined objects with arbitrarily chosen spectrum (square, circle, triangle). Each scene is rendered as a full multispectral light field for all possible parameter combinations, as described in Section 3, for the ideal scenario of fully flat layouts as well as the more realistic case with object depth (and hence only approximately constant disparity), ranging from a few millimeters (CD, Lemons) to sev-

(a) *CD.* (b) *Colorchart.* (c) *Concrete.*

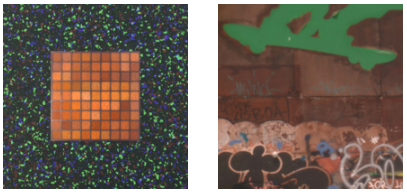

(d) *Curry.* (e) *Graffiti.*

Figure 2: The used scenes (central view) in RGB representation.

eral centimeters (colorcharts, geometric objects). In total, 135 multispectral light fields were rendered for the evaluation, using 16 color channels in the visible spectrum. The multispectral light fields are then spectrally coded in the (s,t)-coordinate by applying the filter mask according to (1). We perform the evaluation using a random and a regular mask. Using a random mask, for every microlens (s,t) a random wavelength index is independently drawn from a discrete uniform distribution $\mathcal{U}(1,\Lambda)$. In the regular case, the mask consists of a regular 4×4 px macropixel containing every wavelength index exactly once. The reconstructed multispectral image can then be quantitatively evaluated: For every parameter set and scene, we calculate the amount a_{rec} of reconstructed pixels and the reconstruction quality given by the peak signal-to-noise ratio (PSNR) between the original light field's central view and the reconstructed multispectral image using either a random or a regular filter mask. For the ideal case of completely flat scenes, we denote the reconstruction quality by PSNR_i whereas for the case with realistic object depth PSNR_r is used. Due to the different object distances, the rendered scenes will show slightly different fields of view (FOV). To perform a fair comparison, the PSNR of every reconstruction is calculated on the region of the image that is shared by all scenes: For the smallest object distance g across the different camera parameters, we calculate a reference FOV and, for scenes with larger g, the region in the rendered image that corresponds to the narrower FOV by simple geometric relations. In this way, every PSNR is calculated on the same image content (but with varying image resolution).

5 Results

First, we found that using multiple, different random masks for the reconstruction of one specific scene only showed a standard deviation of about 0.1 dB in the reconstruction PSNR. Therefore, for the remaining evaluation, we only consider one random mask per reconstructed image. However, in order to increase the statistical significance, we use a different random mask for every reconstruction.

Second, from Figure 3, we observe that, using a regular mask, the reconstruction performs very well for even integer valued disparities but poorly for odd ones. Since the regular mask is of size 4×4 px, this is easily understood: Every imaged point of the scene only passes every d-th filter, for example, in the case where the disparity is $d = 2$, the point passes every other and hence only 4 of the total 16 color filters. Therefore, the performance of the reconstruction for the regular mask depends on whether the disparity is a true divisor of the size of the regular filter's macropixel. This makes the regular mask unsuitable for generalization and adaption to different disparities. For this reason, we are only considering the random mask for the remaining evaluation.

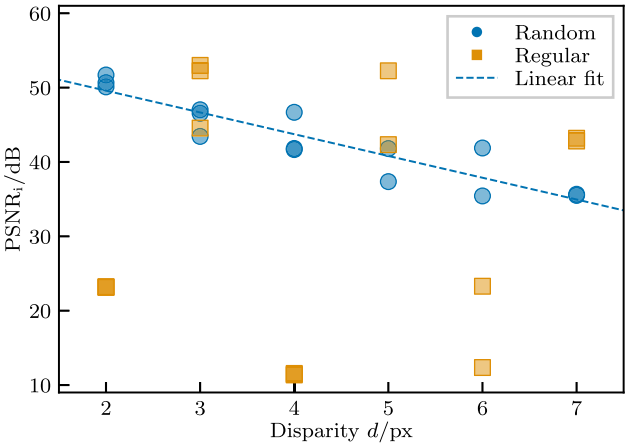

Figure 3: Average reconstruction quality across all scenes for different coding masks and disparities.

In general, we find very high reconstruction qualities, as shown in Figure 3 and in more detail in Table 1. Overall, the smaller the disparity, the higher the reconstruction quality. This, in fact, is not due to the disparity itself, but due to the number of possible subapertures compatible with that disparity. In general, smaller disparity values correspond to a larger number of subapertures under the constraints proposed in Section 3. With more

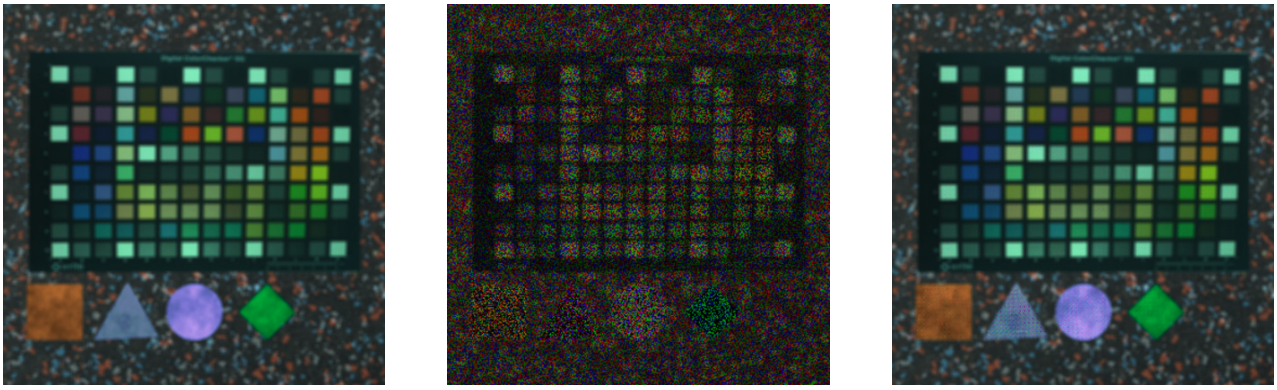

(a) Center view of original (left) respectively spectrally coded light field (middle) and reconstructed multispectral image in RGB (right).

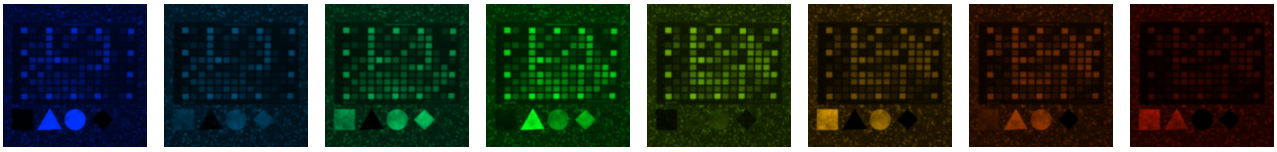

(b) Every other, thus 8, of the 16 reconstructed color channels from 400 nm (left) to 700 nm (right),

Figure 4: Reconstruction of scene *Colorchart* with $F = 1.4$, $d = 4$ px, $N = 7$ and random filter mask. $\mathrm{PSNR_r} = 38.96$ dB.

Table 1: Average reconstruction quality across all scenes for all parameter combinations in case of a random filter mask.

F	d/px	N	a_{rec}/%	$\mathrm{PSNR_i}$/dB	$\mathrm{PSNR_r}$/dB
1.4	2	13	**99.93**	**51.70**	**47.92**
1.4	2	11	99.70	50.10	47.13
1.8	2	11	99.69	50.66	47.25
1.4	3	11	99.63	43.44	42.29
1.8	3	9	98.18	47.02	43.37
1.4	3	9	98.17	46.55	43.41
1.4	4	9	98.07	46.68	42.60
1.4	4	7	91.86	41.67	38.96
1.8	4	7	91.85	41.82	39.15
1.8	5	7	91.72	37.36	36.37
1.4	5	7	91.71	41.80	38.88
1.4	6	7	91.55	41.88	38.86
1.8	6	5	73.54	35.43	33.57
1.8	7	5	73.45	35.66	33.59
1.4	7	5	73.44	35.50	33.72

available subapertures, the amount of reconstructed pixels, and therefore the reconstruction quality, naturally increases.

Changing from ideally flat to real scenes, we find an average drop in the PSNR of about 2.7 dB as shown in Table 1. A reconstruction of the scene *Colorchart* is shown in more detail in Figure 4. Note that, since the camera is focused at infinity and due to the large f-number and small number of subapertures, the effective aperture size is quite large and the image is slightly blurry. Furthermore, we do observe some artifacts in the reconstruction of the artificial geometric objects. These are specified using a narrow spectral signature. Hence, the linear 1D interpolation that is used to interpolate the remaining missing pixels is unsuited in this case. Here, using a 2D spatial interpolation should give better results.

Concluding, the reconstruction quality is very high, but, as usual, there is a trade-off between many camera parameters: choosing a smaller number of subapertures leads to a higher subaperture resolution but a narrower depth of field and a slightly worse reconstruction PSNR. Since the camera is focused at infinity, this causes blur in the recorded light field due to a large effective aperture size. Choosing a larger number of subapertures leads to very high reconstruction PSNR and a wider depth of field but increases the redundancy of spectral information. Furthermore, the reconstruction of course also depends on the chosen number of color channels. Given a specific application, the optimal parameter combination can be chosen according to self-defined criteria and the results shown in Table 1. To perform the evaluation for a different specific application, we make the source code (parameter creation, scene synthesis, evaluation) publicly available at [9].

The potential speed of the imaging system is presumably very high. The reconstruction of the multispectral image is performed using only a very basic pixel shifting (in case of integer valued disparities) and could easily be implemented in a real-time capable fashion. The bottleneck

with respect to speed is the decoding of the coded light field $\hat{L}(u, v, s, t; \lambda)$ from the 2-D sensor image. For this, multiple calibration and decoding schemes are presented in the literature [6, 5]. Given the corresponding hardware and optimized implementation, the decoding of the sensor image should be possible with high frame rates, depending on the sensor resolution. Raytrix light field cameras, according to the vendor's product sheets, can reach frame rates from about 7 Hz up to 330 Hz using a GPU optimized decoding, supporting the above claim.

6 Conclusion

We have proposed a new method to reconstruct multispectral images from spectrally coded light fields for a camera with spectrally coded microlens array and focused at infinity. For different camera parameter sets suited for real-case scenarios such as in-line production monitoring, we achieve reconstruction PSNRs of up to 51 dB. The shown evaluation may help optimize a camera parameter set for a given measurement task. For easy adaption, we provide the source code of all necessary steps [9].

Furthermore, the proposed method is easily generalized to super-resolution methods: by choosing half-integer valued disparities, shifting the subapertures onto a target with doubled resolution, a reconstruction of a super-resolved multispectral image is possible. First evaluations showed a reconstruction of up to 80 % of the target's pixels. This shall be addressed in future evaluations.

Finally, the presented methods might support the reconstruction of the full underlying multispectral light field, e. g. supporting methods from compressed sensing and sparse representation.

As compared to other multispectral snapshot imagers, the spectrally coded light field camera can be build in a compact, robust, monocular design. In this aspect, it only competes with multispectral snapshot imagers using a spectrally coded sensor [7]. Since our approach basically corresponds to a miniaturized multi-camera setup, the multispectral image's quality, compared to spectrally coded sensors, is expected to be higher. Essentially, our approach is non-compressive and does not rely on interpolation. Hence, spatial discontinuities such as edges are reconstructed with higher quality. A quantitative evaluation of these claims is left for future work.

Acknowledgment: The authors acknowledge support by the state of Baden-Württemberg through bwHPC, a massively parallel computer.

References

1. E. H. Adelson and J. Y. A. Wang. Single lens stereo with a plenoptic camera. *IEEE Transactions on Pattern Analysis and Machine Intelligence*, 14(2):99–106, 1992.
2. J. Anastasiadis and F. Puente León. Detection of substances in food with 3D convolutional autoencoders. *tm – Technisches Messen*, 85(1):38–44, 2018.
3. B. Arad and O. Ben-Shahar. Sparse recovery of hyperspectral signal from natural RGB images. In *IEEE European Conference on Computer Vision*, pages 19–34. Springer, 2016.
4. K. Berkner and S. Shroff. Optimization of spectrally coded mask for multi-modal plenoptic camera. In *Imaging and Applied Optics*, page CMD4, 2011.
5. Y. Bok, H.-G. Jeon, and I. S. Kweon. Geometric calibration of micro-lens-based light field cameras using line features. *IEEE Transactions on Pattern Analysis and Machine Intelligence*, 39(2):287–300, 2017.
6. D. G. Dansereau, O. Pizarro, and S. B. Williams. Decoding, calibration and rectification for lenselet-based plenoptic cameras. In *Proceedings of the IEEE conference on computer vision and pattern recognition*, pages 1027–1034, 2013.
7. B. Geelen, N. Tack, and A. Lambrechts. A compact snapshot multispectral imager with a monolithically integrated per-pixel filter mosaic. In *Advanced Fabrication Technologies for Micro/Nano Optics and Photonics VII*, volume 8974, page 89740L. International Society for Optics and Photonics, 2014.
8. R. Horstmeyer, G. Euliss, and R. Athale. Flexible multimodal camera using a light field architecture. In *IEEE International Conference on Computational Photography*, pages 1–8, 2009.
9. Institute of Industrial Information Technology, Karlsruhe Institute of Technology. Public GitLab repositories. https://gitlab.com/iiit-public, GNU GPLv3 License, 2019.
10. W. Krippner, S. Bauer, and F. Puente León. Optical determination of material abundances in mixtures. *tm – Technisches Messen*, 84(3):207–215, 2017.
11. G. Lu and B. Fei. Medical hyperspectral imaging: a review. *Journal of Biomedical Optics*, 19(1):010901, 2014.
12. R. Lu and Y.-R. Chen. Hyperspectral imaging for safety inspection of food and agricultural products. In *Pathogen Detection and Remediation for Safe Eating*, volume 3544, pages 121–134. International Society for Optics and Photonics, 1999.
13. A. Lumsdaine and T. Georgiev. The focused plenoptic camera. In *IEEE International Conference on Computational Photography*, pages 1–8, 2009.
14. R. Ng, M. Levoy, M. Brédif, G. Duval, M. Horowitz, and P. Hanrahan. Light field photography with a hand-held plenoptic camera. *Computer Science Technical Report*, 2(11): 1–11, 2005.
15. T. Nürnberg, M. Schambach, D. Uhlig, M. Heizmann, and F. Puente León. A simulation framework for the design and evaluation of computational cameras. In *Proceedings of SPIE Automated Visual Inspection and Machine Vision III*, 11061, 2019.
16. P. Tatzer, M. Wolf, and T. Panner. Industrial application for inline material sorting using hyperspectral imaging in the NIR range. *Real-Time Imaging*, 11(2):99–107, 2005.
17. D. Uhlig and M. Heizmann. Multi-stereo deflectometry with a light-field camera. *tm – Technisches Messen*, 85(1):59–65, 2018.

18. S. Wanner and B. Goldluecke. Variational light field analysis for disparity estimation and super-resolution. *IEEE transactions on pattern analysis and machine intelligence*, 36(3):606–619, 2013.
19. Z. Xiong, L. Wang, H. Li, D. Liu, and F. Wu. Snapshot hyperspectral light field imaging. In *IEEE Conference on Computer Vision and Pattern Recognition*, pages 6873–6881, 2017.
20. F. Yasuma, T. Mitsunaga, D. Iso, and S. K. Nayar. Generalized assorted pixel camera: postcapture control of resolution, dynamic range, and spectrum. *IEEE Transactions on Image Processing*, 19(9):2241–2253, 2010.
21. J. Ye and F. Imai. High resolution multi-spectral image reconstruction on light field via sparse representation. In *Imaging Systems and Applications*, pages IT3A–4, 2015.
22. Y. Zhang, H. Lv, Y. Liu, H. Wang, X. Wang, Q. Huang, X. Xiang, and Q. Dai. Light-field depth estimation via epipolar plane image analysis and locally linear embedding. *IEEE Transactions on Circuits and Systems for Video Technology*, 27(4):739–747, 2017.
23. K. Zhu, Y. Xue, Q. Fu, S. B. Kang, X. Chen, and J. Yu. Hyperspectral light field stereo matching. *IEEE Transactions on Pattern Analysis and Machine Intelligence*, page 1, 2018.

Bionotes

Maximilian Schambach
Karlsruhe Institute of Technology, Institute of Industrial Information Technology, Karlsruhe, Germany
schambach@kit.edu

Maximilian Schambach recieved his B.Sc. and M.Sc. degree in Physics from the Friedrich Schiller University Jena in 2013 and Leipzig University in 2016, respectively. He is currently working as a research associate at the Institute of Industrial Information Technology (IIIT) at the Karlsruhe Institute of Technology, Germany, where he is pursuing a PhD. degree. His current research interests include signal and image processing, computational imaging and compressed sensing.

Fernando Puente León
Karlsruhe Institute of Technology, Institute of Industrial Information Technology, Karlsruhe, Germany
fernando.puente-leon@kit.edu

Fernando Puente León is a Professor with the Department of Electrical Engineering and Information Technology at Karlsruhe Institute of Technology, Germany, where he heads the Institute of Industrial Information Technology (IIIT). From 2001 to 2002, he was with DS2, Valencia, Spain. From 2002 to 2003, he was a Postdoctoral Research Associate with the Institut für Mess- und Regelungstechnik, University of Karlsruhe. From 2003 to 2008, he was a Professor with the Department of Electrical Engineering and Information Technology, Technische Universität München, Germany. His research interests include image processing, automated visual inspection, information fusion, measurement technology, pattern recognition, and communications.